Biochimica et Biophysica Acta 1838 (2014) 1068–1073

Contents lists available at ScienceDirect

Biochimica et Biophysica Acta

journal homepage: www.elsevier.com/locate/bbamem

Computational and experimental analysis of drug binding to the Influenza M2 channel ☆

Raphael Alhadeff [1], Dror Assa [1], Peleg Astrahan [2], Miriam Krugliak, Isaiah T. Arkin *

Department of Biological Chemistry, The Alexander Silberman Institute of Life Sciences, The Hebrew University of Jerusalem, Edmund J. Safra Campus, Jerusalem 91904, Israel

ARTICLE INFO

Article history:
Received 5 June 2013
Received in revised form 22 July 2013
Accepted 25 July 2013
Available online 7 September 2013

Keywords:
Channel blocker
Cell based assay
Anti-flu agent
Potential of mean force

ABSTRACT

The Influenza Matrix 2 (M2) protein is the target of Amantadine and Rimantadine which block its H^+ channel activity. However, the potential of these aminoadamantyls to serve as anti-flu agents is marred by the rapid resistance that the virus develops against them. Herein, using a cell based assay that we developed, we identify two new aminoadamantyl derivatives that show increased activity against otherwise resistant M2 variants. In order to understand the distinguishing binding patterns of the different blockers, we computed the potential of mean force of the drug binding process. The results reveal that the new derivatives are less mobile and bind to a larger pocket in the channel. Finally, such analyses may prove useful in designing new, more effective M2 blockers as a means of curbing influenza. This article is part of a Special Issue entitled: Viral Membrane Proteins — Channels for Cellular Networking.

1. Introduction

The *Influenza A* virus is an RNA virus of the *Orthomyxoviridae* family, giving rise to widespread seasonal epidemics and, less frequently, to severe pandemics. While the seasonal epidemics have low mortality rate, past pandemic events caused heavy losses in human lives. Among these is the Spanish flu (1918), which killed 2–20% of those infected, with an infection rate as high as 50%. Later, smaller outbreaks such as the Asian flu (1957) and Hong Kong flu (1968) claimed the lives of millions, and in 2009, the H1N1 swine flu became a prominent illness causing agent in children and adults (ages 5–60) [1].

The Matrix 2 (M2) protein is a critical component of the *Influenza A* virus. Residing in the virus membrane, its 97 amino acid long sequence encompasses a 19-residue hydrophobic transmembrane domain (TM; residues 25 through 43) and undergoes tetramerization, forming a pore. The pore functions as an ion-channel, selectively allowing an influx of H^+s during cell infection and acidification of the virus lumen [2–4]. The M2 channel is a member of a group of viral proteins which enable membrane permeabilization and are involved in the viral pathogenicity, referred to as *Viroporins*. Other small hydrophobic proteins that are included in the group are HIV-1's Vpu, hepatitis C virus' p7 and HRSV's SH proteins [5,6].

Over the recent years, several structures of the M2 channel have been published, using NMR methods as well as X-ray crystallography, mostly by the groups of Chou, Cross and DeGrado (for example, see [7–10]). Although each structure is slightly different from one another, they all exhibit the same basic topology of a tetramer composed of tilted helices. Smaller details, including the tilt angle itself, vary from structure to structure, and an attempt to compare three of the structures has been done in the past [11].

The channel has been the subject of extensive research, as well as the target of anti-viral agents. The most prevalent drugs that target the channel's activity are Amantadine and Rimantadine, sold commercially as Symmetrel and Flumadine, respectively. However, use of these drugs had led to the development of resistant strains of the virus, and both drugs are currently not recommended as treatment options as anti-flu therapy [12,13].

Among the most prominent resistance-conferring mutations are the substitutions of Ser31 to Asn (S31N) [14] and Val27 to Ala (V27A), the former being present in the resistant swine flu strain. Additional mutations in other pore-lining residues, such as Ala30 and (rarely) Gly34 have also been reported as resistance conferring [15,16]. Previous works suggested that these mutations cause changes in the pore radius thus either interfering with the binding of the drug or rendering the binding futile [17].

In order to better understand the mechanism of H^+ conductance and resistance acquirement by the channel, various electrophysiological methods have been implemented, though some were difficult to carry out due to the acidic environment required to activate the channel [18,19]. Other studies made use of the consequence of the channel activity in order to indirectly measure it. In a method introduced by us in 2011 [20], the channel is heterologously expressed in bacteria, having

☆ This article is part of a Special Issue entitled: Viral Membrane Proteins — Channels for Cellular Networking.

* Corresponding author.
E-mail address: arkin@huji.ac.il (I.T. Arkin).
[1] These authors contributed equally to the work.
[2] Present address: Israel Oceanographic and Limnological Research, Yigal Allon Kinneret Limnological Laboratory, Migdal, Israel.

0005-2736/$ – see front matter © 2013 Elsevier B.V. All rights reserved.
http://dx.doi.org/10.1016/j.bbamem.2013.07.033

a deleterious effect on the bacteria's growth. The growth inhibition is alleviated when an effective blocker of the channel is provided. A very similar system, differing principally by the choice of chimeric construct, was introduced by Inouye and co-workers in 2013 [21].

In the current study, we scanned a small library of candidate molecules using our bacterial cell-based assay, with the goal of finding an inhibitor to the resistant M2 S31N strain. Two molecules exhibiting such a property were found, and in this study we examine the mechanism of their inhibition by molecular dynamics (MD) simulations.

2. Results and discussion

2.1. Cell based assay for channel blockage

In pursuance of putative inhibitors of the M2 channel, a system for high throughput screening of molecules was established in our group in 2011, based on a bacterial assay [20]. A library of compounds was applied to channel-expressing *Escherichia coli*, while their growth was monitored by measuring $O.D._{600}$ over time.

When the channel protein is inserted into the plasma membrane, it facilitates an influx of H^+s through the cellular membrane and consequent growth retardation of the bacteria. Induction efficiently inhibits the growth, resulting in two-fold growth retardation, or lower (see Fig. 1). Accordingly, screening of potential channel blockers may be achieved by adding various compounds to the growth media and monitoring growth enhancement, as successful blockers of the channel should allow better bacterial growth.

2.2. Novel potential channel blockers

Among a limited number of compounds tested, two exhibited significant rescue of the bacterial growth, hinting that they might act as efficient inhibitors of the M2 channel (see Fig. 2c and d). While other compounds, applied at the same concentration as Rimantadine, either had no effect on growth (growth curves resemble those of *No drug*; data not shown), or had minor effect on the Rimantadine-sensitive Singapore *Influenza A* strain channel. The two new compounds alleviated growth to a higher extent than Rimantadine, in both the Singapore strain (Fig. 1a) and in the resistant swine flu's M2 channel (Fig. 1b), which contains the S31N mutation [22]. This implies that the H^+ flux into the bacterial cell has decreased appreciably due to the presence of the new compounds.

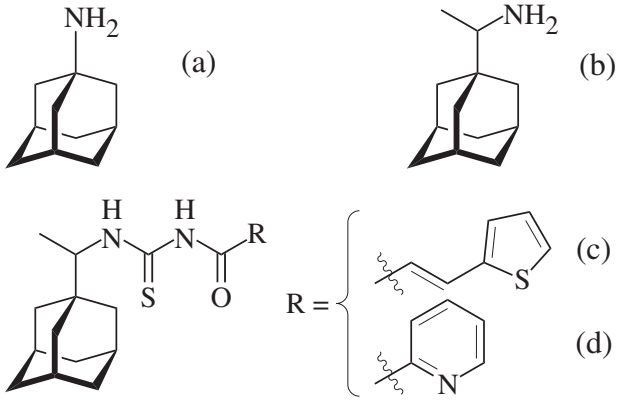

Fig. 2. Known and putative inhibitors of the M2 channel: (a) Amantadine, (b) Rimantadine, (c) Thiophene derivative, and (d) Pyridine derivative.

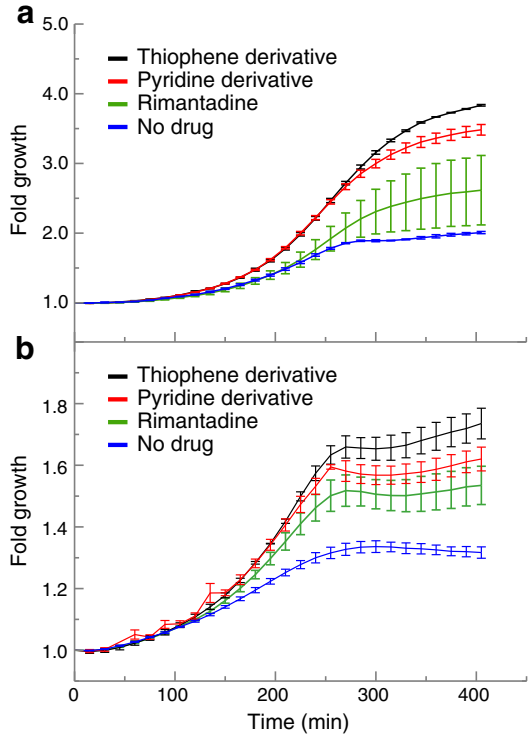

Fig. 1. Growth curves of transformed bacteria expressing the M2 channel from the Singapore strain (a) or the swine flu (b). The different curves correspond to treatments of different M2 blockers, as indicated. Growth was normalized in relation to the initial value.

2.3. Assessment of the compounds' EC50 and toxicity on bacteria

Based on the initial results from the chemical screening, we conducted an experiment to assess the effectiveness of the newly found compounds. Using the same expression system mentioned above, we added each compound in two-fold serial dilutions, varying from 0.8 μM to 50 μM final concentrations, to the growth media of the resistant swine flu M2 expressing bacteria. Additionally, we tested the compounds' toxicity upon the bacteria, by applying the same concentrations on un-induced bacteria. The compounds did not diminish the bacterial growth rate, as well as the final bacterial density (data not shown). Taken together we can conclude that the new compounds exhibited no toxicity towards the bacteria.

While Rimantadine could not rescue the growth of bacteria expressing the swine flu's M2 channel, both of the new compounds significantly

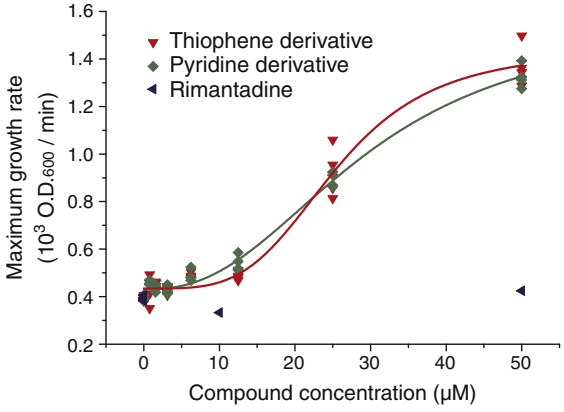

Fig. 3. Maximal growth rate of bacteria treated with the Pyridine derivative, the Thiophene derivative or Rimantadine. The smooth lines depict the fitted function for dose–response relationship of the Pyridine derivative or the Thiophene derivative.

improved the growth rate and the final bacterial densities, relative to the untreated bacteria (Fig. 3). Note that the growth rates in the presence of the new compounds did not reach the un-induced bacteria's maximal growth rate, suggesting that the growth inhibition was not fully alleviated even in concentrations as high as 50 μM. To quantitate the effect the compounds have had on the bacterial population, a dose–response curve was fitted to the data, yielding $EC50 = 25.4 \pm 1.3$ μM for the Thiophene derivative and $EC50 = 29.5 \pm 2.7$ μM for the Pyridine derivative.

2.4. Computational analysis of drug binding

In order to better understand the mode of inhibition, we performed atomistic molecular dynamics simulations of Rimantadine and its Pyridine and Thiophene derivatives binding to the M2 channels. Simulations were performed on the TM-domain of a Rimantadine-sensitive strain (referred to as *RS* throughout the manuscript) and of the resistant S31N mutant-strain. At first, both channels were simulated for 100 ns without any drug and maintained a tetramer structure that did not deviate appreciably from the starting configuration (backbone RMSD ca. 3 Å and no significant deviation in the radius of gyration; see Fig. 4).

Following the simulation of the free channels, we looked into the behavior of the channels and of the drug, using either Rimantadine, Pyridine derivative or Thiophene derivative bound to the RS or resistant M2 channels. We performed umbrella sampling, *i.e.* we ran many short simulations of the drug bound all along the pore axis, from the extracellular water bulk (N-terminus side, designated '*up*') to the intracellular water bulk (C-terminus side, designated '*down*'). In these simulations, we could see the behavior of the protein and of the drug given a particular vertically fixed binding location (as well as the resulting energy profiles, as expanded below).

Throughout the simulations, the drugs fluctuated slightly within the pore, mostly maintaining an overall linear topology and a parallel orientation with their longest axis stretched and aligned with the pore axis. As for the protein, the overall structure was maintained. However, when the drug was adjacent to the lower residues, namely His37 and Trp41, the steric restraints forced the helices to tilt, causing the channel to switch from a cylindrical shape to a conical-'teepee-like' shape. This behavior is expected as these residues are very bulky and do not allow much space for anything else within the pore. Nonetheless, this occurrence might not be so frequent in effect since, as the energies below suggest, the drug should bind higher up in the pore (in the N-terminal direction).

2.4.1. Orientation of the drugs in the channel pore

In order to quantitate the above observation, we analyzed the direction to which the amine group of Rimantadine was pointing, as a function of the position of the drug within the pore. Two main modes for Rimantadine were observed: *upward facing*, with the amine pointing towards the N terminus (extracellular bulk); and *downward facing*. Rimantadine is small enough to rotate freely within the pore, and therefore spontaneous interconversion between the two modes was expected. However, the drug was rarely found to be in any 'in-between' orientation (the amine group pointing orthogonally to the pore axis).

In Fig. 5 the density of sampling Rimantadine in its full upward facing orientation is higher, as long as the drug binds the channel above residue His37. This bias is lost once the drug leaves the pore and enters the extracellular bulk (right end of the graph). When Rimantadine is located below His37 the bias changes to the downward facing orientation, albeit to a lesser extent. Again, Rimantadine has no fixed orientation as it exits to the intracellular bulk (left end of the graph). This behavior may be explained by the fact that Rimantadine is positively charged at physiological pH, and the histidines of M2 have been suggested to be partially charged, with two or three out of the four histidines being positively charged [7,9]. This causes electrostatic repulsion between the histidines and the Rimantadine amine group, forcing it to maintain an orientation that maximizes the distance between the two positively charged groups. This is in line with previously published work by Leonov et al. [17].

We subsequently repeated the same orientational analysis for the Pyridine and for the Thiophene derivatives. However, due to the size of the two derivatives, flipping was not observed in the channel lumen. Therefore, we performed the simulations on these two derivatives in

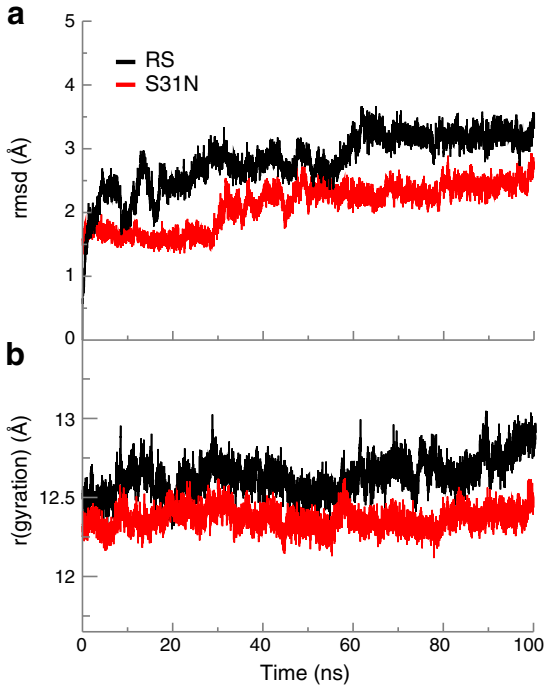

Fig. 4. M2 stability. The backbone RMSD (a) and radius of gyration (b) of the M2 channel throughout the 100 ns simulations of the RS (black) and S31N resistant mutant (red).

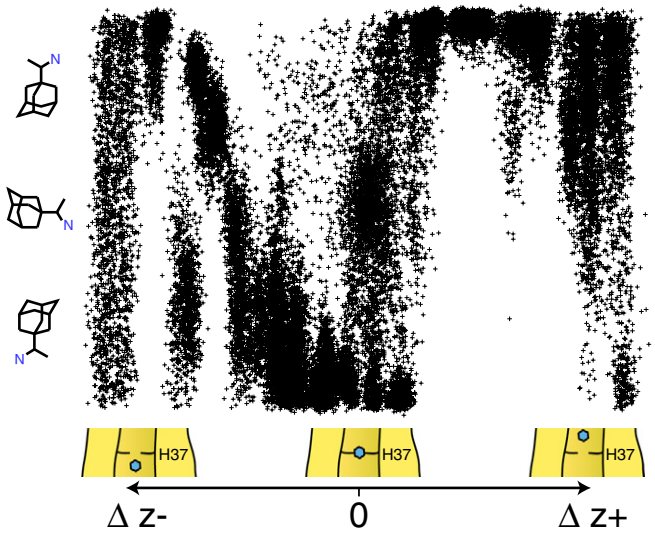

Fig. 5. Rimantadine's amine group direction as a function of the position of Rimantadine along the pore axis of M2 TM domain. The abscissa shows the orientation of the Rimantadine within the pore, 'up' being the amine facing the N-terminus of theM2 protein (the extracellular side). The ordinate presents the location of the Rimantadine along the M2 pore in respect to residue His37: below on the left and above on the right.

both upward and downward facing orientations, to accommodate for the two possibilities of attachment. Considering that both the Pyridine derivative and the Thiophene derivative bear no full charge, there was no reason to assume *a priori* that one orientation would be favorable.

Note that from a chemical point of view, almost the entire molecule, for both compounds, is a conjugated system of delocalized electrons. On top of that, the only rotatable bonds don't produce a substantial change, upon rotation, in the length of the long axis of the molecule, *i.e.* the length and width of the cylinder that makes up the molecule are, in large, constant. It is therefore not surprising that the compounds bind the narrow M2 channel with ease, as they hardly lose entropy upon binding.

2.4.2. Potential of mean force analysis

The umbrella sampling set of shorter simulations described above was collected and unbiased using the WHAM method [23], to compute the free energy profile of the drugs within the channel (a.k.a. potential of mean force or PMF). The PMF profiles were calculated for Rimantadine, Pyridine derivative and Thiophene derivative, in both RS, and resistant strains, as seen in Fig. 6. The profile for Rimantadine in the RS channel exhibits a typical binding curve with a binding site adjacent to residues 27 and 31, a binding site previously reported both structurally [24,25] and computationally [17]. However, when residue Ser31 is mutated to Asn, a well known mutation that confers resistance to known drugs [14], the binding trough is diminished and the energies for binding the channel increase overall. This suggests that the drug does not bind well and is in line with a model previously suggested [17] and supported by experimental results [26]. Note that the free energy increases rapidly as the drug tries to cross His37, probably to accommodate for the electric repulsion.

Examination of the newly found compounds presents a different picture. Focusing on the upward facing PMFs, mimicking the binding orientation of Rimantadine throughout most of the coordinate, a binding site appears roughly at the same location as for Rimantadine, near residues 27 and 31, as well as an energy barrier near His37. In the RS strain, a second binding site near Leu40, which is at the edge of the pore, can be seen. The compounds, which are much larger than Rimantadine, allow more interactions through the non-adamantyl portion, probably allowing the formation of the second binding site.

Moving on to the S31N resistant mutant, the curves present an energy profile where the second binding site is replaced by an energy barrier. Interestingly, the first 'Rimantadine-like' binding site is present and is mostly unchanged. This could explain why these compounds are still able to inhibit M2 S31N strains, albeit not to the same extent they inhibit the RS channel.

Looking at the PMFs of the downward facing orientation, the differences in energies are surprisingly not as dramatically different as one might expect. For the case of the Pyridine derivative compound binding the RS strain, the binding energies seem to be highly similar to the upward facing orientation energies, but the energy barrier seems to be much lower, suggesting that the downward facing binding is energetically favorable. Binding to the S31N mutant introduces a new energy barrier near Val27. In this case, we expect that the binding of the compound in downward facing orientation will be less common, but more long lasting, since the energy trough is situated between two high peaks. This would imply a lower k_{on} and k_{off}, with no clear conclusion on the difference in K_d.

In the case of the Thiophene derivative compound, we cannot detect a principal difference for the S31N mutant; however, the curve for the downward facing binding to the RS strain is intriguing: the energy profile presents energy barriers that are smaller than previously discussed energy barriers (by at least 5 k_BT) on both sides of a novel binding site situated near Gly34. Kinetically, even though this binding trough is as deep as the binding troughs of the upward facing curve, it is expected to be seldom visited because the funnel entry is narrow. In other words, the energetically preferred route to the binding site demands the compound's upward position, arguing statistical unlikelihood of the downward position's binding.

While the energy profiles may explain binding of the compounds to M2, the question of how they actually inhibit the channel remains open. Rimantadine was previously suggested to inhibit the proton flux by simple charge repulsion [17], and indeed we were able to reproduce these results (data not shown). However, we do not see the same focused positive electrostatic potential for the uncharged Pyridine derivative and Thiophene derivative. This raises an interesting conclusion that M2 may be inhibited in more than one way. The inhibition could be explained by steric hindrance, being more bulky than the smaller Rimantadine, or by limiting protein flexibility and attached water, which might interfere with H^+ conductance. However, further clarification on the modes of inhibition will require more research.

To conclude, the PMF profiles suggest that, in contrast to Rimantadine, which does not bind the S31N mutant appreciably, the compounds we present maintain some form of binding. This might be due to the existence of two modes of binding (or more, if considering the downward facing modes of binding) which are not fully abolished by the resistance conferring mutation (a representative snapshot of one such mode of binding is shown in Fig. 7). This should explain why the Pyridine derivative and the Thiophene derivative show some sort of inhibition on the resistant mutant S31N. This presents an encouraging turning point towards the development of drugs that will be effective against resistant seasonal influenza outbreaks.

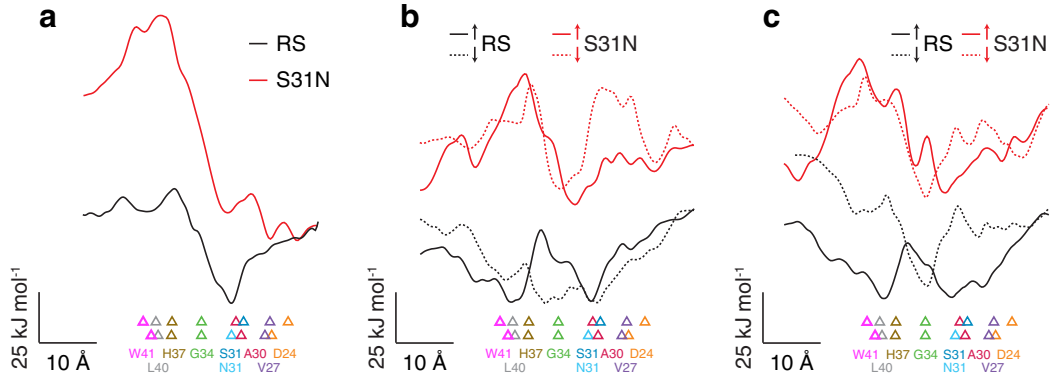

Fig. 6. The potential of mean force of the various drugs along the M2 pore axis. The free energy profile of the RS channel is in black, while that of the S31N resistant mutant is in red. For the compounds, full lines represent the upward facing orientation and the dashed lines represent the downward facing orientation. The triangles present the average coordinate of the side-chain of the indicated residue; top triangles belong to the resistant mutant, bottom triangles belong to the RS strain. The scales are presented on the bottom left corner. (a) Rimantadine; (b) Pyridine derivative; (c) Thiophene derivative.

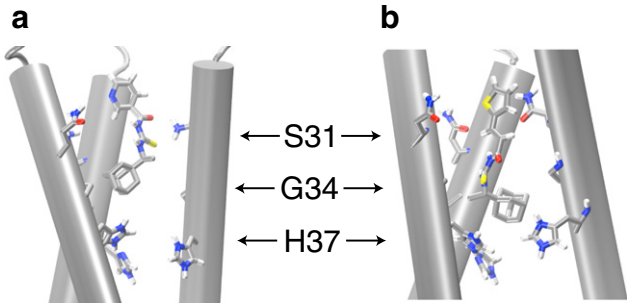

Fig. 7. A representative snapshot of the compounds bound in an upward facing conformation, in the S31N M2 channel. The front helix of the M2 bundle was removed for better visualization. The Pyridine derivative is shown in panel a and Thiophene derivative in panel b.

3. Materials and methods

3.1. Chemicals

1-Aminoadamantane (Amantadine) and racemic 1-(1-adamantyl)-ethanamine (Rimantadine) were purchased from Sigma-Aldrich laboratories. N-(((1-(1-adamantyl)ethyl)amino)carbonothioyl)-3-(2-thienyl) acrylamide (Thiophene derivative, compound 5197035) and N-(((1-(1-adamantyl)ethyl)amino)carbonothioyl)-nicotinamide (Pyridine derivative, compound 5150923) were purchased from ChemBridge Corporation (San Diego, CA) and were dissolved in DMSO to a concentration of 5 mM; for chemical structures of the compounds, see Fig. 2. Isopropyl-β-D-thio-galactopyranoside (IPTG) was purchased from Biochemika-Fluka (Buchs, Switzerland). The pMal-p2x vector was purchased from New England Biolabs (Ipswich, MA). DH10B *E. coli* cells were purchased from Invitrogen (Carlsbad, CA).

3.2. Plasmids and bacterial strains design

The Singapore M2 sequence was synthesized *via* a multistep PCR protocol. This RS construct was designed according to the Singapore H2N2 isolate, M2 sequence [15], and was inserted into pMal-p2x using the methods stated in [20] so it was in frame to the carboxy-terminus of the MalE protein, following a poly-Asn site. The plasmid was inserted into *E. coli* of the DH10B strain. The swine flu strain [27] was obtained through point mutations on the Singapore strain with the Quick multi-Mutagenesis kit from Stratagene (La Jolla, CA).

3.3. Bacterial growth

Cells bearing or lacking (as a control) the ion channel genes were incubated overnight in LB with 100 μg/ml Ampicillin. Thereafter, the growth culture was diluted 100 fold and the bacteria were grown until their $O.D._{600}$ reached 0.07–0.1. Cells were then divided into 96 well flat-bottomed plates (from Nunc, Roskilde, Denmark) containing the different treatments. The growth volume in each well was 100 μl. In the chemical screening assay, IPTG to a final concentration of 60 μM was added to the cells; in the dose–response assays, IPTG concentration was 35 μM in *High induction* experiments, or ≤17.5 μM in *Low induction* experiments. D-glucose was added, to a concentration of (1%). The final concentration of DMSO was 1%. 96 well plates were incubated for 16 h at 30 °C in a Synergy 2 multi-detection micro-plate reader from BioTek (Winooski, VT), or in Infinite 200 from Tecan Group (Männedorf, Switzerland) at a constant *high* shaking rate. $O.D._{600}$ readings were recorded every 15 min. For every measurement, duplicates or more were done.

3.4. Dose–response relationship

Effective-concentration of 50% (*EC*50) was derived by measuring the dose–response effect of the Pyridine derivative or the Thiophene derivative upon the maximal growth rate of the channel-expressing bacteria. To the resulting data we non-linearly fit a curve according to the equation relating the maximal growth rate (R) to the drug concentration:

$$y = R_0 + \frac{R_{max} - R_0}{1 + \left(\frac{R}{EC50}\right)^n}$$

where R_0 is the maximal growth rate without a drug, R_{max} is the maximal growth rate when all growth-inhibition is lifted, and n is the maximal slope of the curve.

3.5. Molecular dynamics

For the simulation system of the RS M2, we used the recent X-ray structure of the M2's TM domain tetramer, taken from the PDB (PDB ID: 3LBW, [7]). We reverted residue 34 to *wt* Gly; the N-termini were capped with acetyl groups, and crystallographic water molecules were kept in the system.

For the simulation system of the resistant M2, we used the structure of the S31N mutant solved by NMR (PDB ID: 2LY0, [10]). We clustered the 20 structures together using *g_cluster* from the GROMACS package [28,29], using a cutoff that would include all 20 structures in the same cluster, and the frame that was the closest (by RMSD) to the representative structure was chosen. The drug molecule was removed from the structure, and the N-termini were capped with acetyl groups. In both systems, the protonation pattern for His37 was that of two opposing positively charged histidines.

Next, each of the two systems underwent the following procedure: The system was embedded in a pre-equilibrated DMPC membrane so that the protein is perpendicular to the membrane plane, and all clashing lipids and water molecules within 2 Å of the protein were deleted. The system's charge was neutralized by adding K^+ and Cl^- ions to a final concentration of 140 mM, randomly distributed. The system was then subjected to energy minimization using the steepest descent algorithm, with a tolerance of 1000 $kJ \cdot mol^{-1} \cdot nm^{-1}$, followed by two more steps using the conjugated gradient algorithm, with tolerances of 100 and 10 $kJ \cdot mol^{-1} \cdot nm^{-1}$. After the minimization step, the system was equilibrated by simulating it under positional restraints on the protein (and crystallographic water molecules, if present), with a harmonic force constant of $k = 1000\ kJ \cdot mol^{-1} \cdot nm^{-2}$ for 1 ns. This step was repeated using a force constant of $k = 500\ kJ \cdot mol^{-1} \cdot nm^{-2}$ for 100 ps, and a final step of unrestrained simulation of another 1 ns. The gradual removal of the restraints allowed for the lipids and water molecules to pack more tightly around the protein, preventing the tetramer from breaking apart.

For the structure and topology of the drugs, we used the ATB server [30] to construct initial models of the molecules with partial charges and bonded parameters. The parameters were slightly modified based on chemical considerations as suggested by Professor Silvio E. Biali from the Hebrew University of Jerusalem, Israel (personal communication); bond lengths were fitted to similar known molecules already existing in the GROMACS database (*e.g.* the pyridine group was based on NADH) and several angle rotations were limited to account for resonance and conjugation effects (also in line with reported number of rotatable bonds from ChemBridge). The molecules were then submitted to MD simulations in water for equilibration and parameter validation.

3.6. MD details

The simulations were conducted using the GROMACS package [28,29], employing an extended version of the GROMOS53a6 force field [31]. All simulations were conducted using the LINCS algorithm [32] to

constrain bond lengths and angles of hydrogen atoms, allowing a time step of 2 fs. Simulations were run using Berendsen temperature coupling at 310 K employing a coupling constant of $\tau = 0.1$ ps. Pressure was kept constant at 1 bar by applying semi-isotropic coupling with a coupling constant of $\tau = 1$ ps, differentiating the z axis (the membrane normal). A cutoff of 1.2 nm was used for van der Waals interactions, and long range electrostatic interactions were computed using the PME method [33]. The water model used was SPC [34].

3.7. Potential of mean force (PMF)

We applied umbrella sampling [35] in order to compute the PMF of the various drugs in the pore of the M2 channel. The simulations were composed of the equilibrated M2 channel (RS strain or drug resistant) and an equilibrated drug (Rimantadine, Pyridine derivative or Thiophene derivative). The drug was aligned to the M2 axis and inserted into the pore in such a way that it will not clash with any residue, while clashing water molecules were moved if needed. The various frames were constructed by placing the drug along the z-axis at 2 Å intervals, simulating the system for each position. Additional frames were added to compensate for poor sampling, until the histograms were sufficiently overlapped, making up between 30 and 40 frames for each combination of drug-strain. Each frame was energy minimized using the same parameters as above and then subjected to a 10 ns simulation. The harmonic force was applied to the z-axis only, using a constant of $k = 1000\ \mathrm{kJ \cdot mol^{-1} \cdot nm^{-2}}$. Unbiasing and integration were done using the Weighted Histogram Analysis Method (WHAM) [23].

3.8. Visualization and analysis

The simulations were visualized with the visual molecular dynamics (VMD) program [36]. The analyses were conducted using in-house VMD Tcl scripts, in-house purpose written perl scripts, and the GROMACS analysis package tools. For the image of the bound drug in the M2 channel a frame from the umbrella sampling data set was selected, where the z-coordinate of the drug fits the energy trough.

Acknowledgements

This work was supported in part by grants from The Rudin Fellowship Trust, and grants from the Israeli Science Foundation (1581/08) and the German Israel Foundation. ITA is the Arthur Lejwa Professor of Structural Biochemistry at the Hebrew University of Jerusalem.

References

[1] J.K. Taubenberger, D.M. Morens, 1918 influenza: the mother of all pandemics, Emerg. Infect. Dis. 12 (2006) 15–22.
[2] R.A. Lamb, S.L. Zebedee, C.D. Richardson, Influenza virus M2 protein is an integral membrane protein expressed on the infected-cell surface, Cell 40 (1985) 627–633.
[3] L.H. Pinto, L.J. Holsinger, R.A. Lamb, Influenza virus M2 protein has ion channel activity, Cell 69 (1992) 517–528.
[4] T. Sakaguchi, Q. Tu, L.H. Pinto, R.A. Lamb, The active oligomeric state of the minimalistic influenza virus M2 ion channel is a tetramer, Proc. Natl. Acad. Sci. U. S. A. 94 (1997) 5000–5005.
[5] M.E. Gonzalez, L. Carrasco, Viroporins, FEBS Lett. 552 (2003) 28–34.
[6] J.L. Nieva, V. Madan, L. Carrasco, Viroporins: structure and biological functions, Nat. Rev. Microbiol. 10 (2012) 563–574.
[7] R. Acharya, V. Carnevale, G. Fiorin, B.G. Levine, A.L. Polishchuk, V. Balannik, I. Samish, R.A. Lamb, L.H. Pinto, W.F. DeGrado, M.L. Klein, Structure and mechanism of proton transport through the transmembrane tetrameric M2 protein bundle of the influenza A virus, Proc. Natl. Acad. Sci. U. S. A. 107 (2010) 15075–15080.
[8] R.M. Pielak, J.J. Chou, Solution NMR structure of the V27A drug resistant mutant of influenza A M2 channel, Biochem. Biophys. Res. Commun. 401 (2010) 58–63.
[9] M. Sharma, M. Yi, H. Dong, H. Qin, E. Peterson, D.D. Busath, H.-X. Zhou, T.A. Cross, Insight into the mechanism of the influenza A proton channel from a structure in a lipid bilayer, Science 330 (2010) 509–512.
[10] J. Wang, Y. Wu, C. Ma, G. Fiorin, J. Wang, L.H. Pinto, R.A. Lamb, M.L. Klein, W.F. Degrado, Structure and inhibition of the drug-resistant S31N mutant of the M2 ion channel of influenza A virus, Proc. Natl. Acad. Sci. U. S. A. 110 (2013) 1315–1320.
[11] H. Leonov, I.T. Arkin, Structure and dynamics of the influenza A M2 channel: a comparison of three structures, J. Mol. Model. 15 (2009).
[12] R.A. Bright, D.K. Shay, B. Shu, N.J. Cox, A.I. Klimov, Adamantane resistance among influenza A viruses isolated early during the 2005–2006 influenza season in the United States, JAMA 295 (2006) 891–894.
[13] A.E. Fiore, A. Fry, D. Shay, L. Gubareva, J.S. Bresee, T.M. Uyeki, Antiviral agents for the treatment and chemoprophylaxis of influenza — recommendations of the Advisory Committee on Immunization Practices, Technical Report 1, Centers for Disease Control and Prevention, 2011.
[14] A. Krumbholz, M. Schmidtke, S. Bergmann, S. Motzke, K. Bauer, J. Stech, R. Dürrwald, P. Wutzler, R. Zell, High prevalence of amantadine resistance among circulating European porcine influenza A viruses, J. Gen. Virol. 90 (2009) 900–908.
[15] A.J. Hay, A.J. Wolstenholme, J.J. Skehel, M.H. Smith, The molecular basis of the specific anti-influenza action of amantadine, EMBO J. 4 (1985) 3021–3024.
[16] T.M. Sweet, H.F. Maassab, K. Coelingh, M.L. Herlocher, Creation of amantadine resistant clones of influenza type A virus using a new transfection procedure, J. Virol. Methods 69 (1997) 103–111.
[17] H. Leonov, P. Astrahan, M. Krugliak, I.T. Arkin, How do aminoadamantanes block the influenza M2 channel, and how does resistance develop? J. Am. Chem. Soc. 133 (2011) 9903–9911.
[18] V. Vijayvergiya, R. Wilson, A. Chorak, P.F. Gao, T.A. Cross, D.D. Busath, Proton conductance of influenza virus M2 protein in planar lipid bilayers, Biophys. J. 87 (2004) 1697–1704.
[19] J.A. Mould, J.E. Drury, S.M. Frings, U.B. Kaupp, A. Pekosz, R.A. Lamb, L.H. Pinto, Permeation and activation of the M2 ion channel of influenza A virus, J. Biol. Chem. 275 (2000) 31038–31050.
[20] P. Astrahan, R. Flitman-Tene, E.R. Bennett, M. Krugliak, C. Gilon, I.T. Arkin, Quantitative analysis of influenza M2 channel blockers, Biochim. Biophys. Acta 1808 (2011) 394–398.
[21] L. Mao, J. Wang, W.F. DeGrado, M. Inouye, An assay suitable for high throughput screening of anti-influenza drugs, PLoS One 8 (2013) e54070.
[22] Centers for Disease Control, Prevention (CDC), Update: drug susceptibility of swine-origin influenza A (H1N1) viruses, April 2009, MMWR Morb. Mortal. Wkly Rep. 58 (2009) 433–435.
[23] S. Kumar, D. Bouzida, R. Swendsen, P. Kollman, J. Rosenberg, The Weighted Histogram Analysis Method for free-energy calculations on biomolecules.1. The method, J. Comput. Chem. 13 (1992) 1011–1021.
[24] A.L. Stouffer, R. Acharya, D. Salom, A.S. Levine, L. Di Costanzo, C.S. Soto, V. Tereshko, V. Nanda, S. Stayrook, W.F. DeGrado, Structural basis for the function and inhibition of an influenza virus proton channel, Nature 451 (2008) 596–599.
[25] S.D. Cady, K. Schmidt-Rohr, J. Wang, C.S. Soto, W.F. Degrado, M. Hong, Structure of the amantadine binding site of influenza M2 proton channels in lipid bilayers, Nature 463 (2010) 689–692.
[26] P. Astrahan, I. Kass, M.A. Cooper, I.T. Arkin, A novel method of resistance for influenza against a channel-blocking antiviral drug, Proteins 55 (2004) 251–257.
[27] R.J. Garten, C.T. Davis, C.A. Russell, B. Shu, S. Lindstrom, A. Balish, W.M. Sessions, X. Xu, E. Skepner, V. Deyde, M. Okomo-Adhiambo, L. Gubareva, J. Barnes, C.B. Smith, S.L. Emery, M.J. Hillman, P. Rivailler, J. Smagala, M. de Graaf, D.F. Burke, R.A.M. Fouchier, C. Pappas, C.M. Alpuche-Aranda, H. López-Gatell, H. Olivera, I. López, C.A. Myers, D. Faix, P.J. Blair, C. Yu, K.M. Keene, P.D. Dotson Jr., D. Boxrud, A.R. Sambol, S.H. Abid, K. St George, T. Bannerman, A.L. Moore, D.J. Stringer, P. Blevins, G.J. Demmler-Harrison, M. Ginsberg, P. Kriner, S. Waterman, S. Smole, H.F. Guevara, E.A. Belongia, P.A. Clark, S.T. Beatrice, R. Donis, J. Katz, L. Finelli, C.B. Bridges, M. Shaw, D.B. Jernigan, T.M. Uyeki, D.J. Smith, A.I. Klimov, N.J. Cox, Antigenic and genetic characteristics of swine-origin 2009 A(H1N1) influenza viruses circulating in humans, Science 325 (2009) 197–201.
[28] D. Van Der Spoel, E. Lindahl, B. Hess, G. Groenhof, A.E. Mark, H.J.C. Berendsen, GROMACS: fast, flexible, and free, J. Comput. Chem. 26 (2005) 1701–1718.
[29] H. Berendsen, D. van der Spoel, R. vandrunen, GROMACS – a message – passing parallel molecular-dynamics implementation, Comput. Phys. Commun. 91 (1995) 43–56.
[30] A.K. Malde, L. Zuo, M. Breeze, M. Stroet, D. Poger, P.C. Nair, C. Oostenbrink, A.E. Mark, An automated force field topology builder (ATB) and repository: version 1.0, J. Chem. Theory. Comput. 7 (2011) 4026–4037.
[31] S.W.I. Siu, R. Vácha, P. Jungwirth, R.A. Böckmann, Biomolecular simulations of membranes: physical properties from different force fields, J. Chem. Phys. 128 (2008) 125103.
[32] B. Hess, H. Bekker, H. Berendsen, J. Fraaije, LINCS: a linear constraint solver for molecular simulations, J. Comput. Chem. 18 (1997) 1463–1472.
[33] T. Darden, D. York, L. Pedersen, Particle mesh Ewald: an N-log(N) method for Ewald sums in large systems, J. Chem. Phys. 98 (1993) 10089–10092.
[34] H. Berendsen, J. Postma, W. van Gunsteren, J. Hermans, B. Pullman, Intermolecular Forces: Interaction Models for Water in Relation to Protein Hydration, Reidel, Dordrecht, 1981.
[35] G.M. Torrie, J.P. Valleau, Nonphysical sampling distributions in Monte Carlo free-energy estimation: umbrella sampling, J. Comput. Phys. 23 (1977) 187–199.
[36] W. Humphrey, A. Dalke, K. Schulten, VMD: visual molecular dynamics, J. Mol. Graph. 14 (1996) 33–38.